



HAL
open science

A Non-Linear Space-Angle Multi-Grid Acceleration for the Method of Characteristics in Unstructured Meshes

Gabriele Grassi

► **To cite this version:**

Gabriele Grassi. A Non-Linear Space-Angle Multi-Grid Acceleration for the Method of Characteristics in Unstructured Meshes. Nuclear Science and Engineering, 2006, 155 (2), pp.208-222. 10.13182/NSE07-A2657 . cea-02356008

HAL Id: cea-02356008

<https://cea.hal.science/cea-02356008>

Submitted on 2 Dec 2019

HAL is a multi-disciplinary open access archive for the deposit and dissemination of scientific research documents, whether they are published or not. The documents may come from teaching and research institutions in France or abroad, or from public or private research centers.

L'archive ouverte pluridisciplinaire **HAL**, est destinée au dépôt et à la diffusion de documents scientifiques de niveau recherche, publiés ou non, émanant des établissements d'enseignement et de recherche français ou étrangers, des laboratoires publics ou privés.

A Non-Linear Space-Angle Multi-Grid Acceleration for the Method of Characteristics in Unstructured Meshes

Gabriele Grassi

Commissariat à l'Énergie Atomique

Service d'Études des Réacteurs et de Modélisation Avancée

CEA de Saclay, DM2S/SERMA

91191 Gif-sur-Yvette, France

gabriele.grassi@cea.fr

Total number of pages: 37

Number of Figures: 2

Number of Tables: 6

Abstract

A new space-angle multi-grid technique has been developed to accelerate the free inner transport iterations based upon the Method of Characteristics (MOC). We present a two-level scheme: it consists of a fine level on which the MOC transport calculation is performed and a more coarsely discretised phase space in which a low-order problem is solved as an acceleration step. A flux-volume homogenisation technique is employed to define the coarse-level cross sections. This entails the non-linearity of the scheme. Restriction and prolongation operators are defined between the two levels. After each fine transport iteration, a low-order transport problem is iteratively solved on the homogenised grid. A coarser angular representation is used within a MOC-like framework. We employ discontinuity factors to reconstruct the scalar incoming and outgoing currents on each region of the coarse discretisation. The solution of the above-mentioned low-order problem is used to correct the angular moments of the flux resulting from the previous free transport sweep. A complete description of the low-order operator and of the grid-to-grid transfer operators is given. A further application of the method to the acceleration of outer transport iterations is also presented. In order to test the effectiveness of our method, numerical tests for given benchmarks geometries have been performed. Results are discussed.

1 Introduction

Transport problems for nuclear reactors are multi-group k -eigenvalue problems, usually with up-scattering. The multi-group formalism yields a system of one-group fixed-source equations coupled via fission and group-to-group transfer sources. The Method of Characteristics (MOC), implemented in the TDT solver for the APOLLO2 code [1], provides an iterative solution for the discrete ordinate formulation of the one-group linear transport equation [2]. In the MOC approach, the phase space is discretised as follows: the geometrical domain \mathcal{D} is decomposed into a set of homogeneous regions $\{\mathcal{D}_i\}$ on which a flat-source approximation is done; a set of discrete angular directions and associated weights $\{\Omega_n, \omega_n\}_{n=1,N}$ is chosen. Then, a set of parallel trajectories is tracked for each direction. The method essentially consists of two main equations: a balance equation for the angular flux on each region i , and a propagation equation giving the angular flux leaving the region i in terms of the incoming angular flux and the internal source. The MOC has proved to be an advantageous tool for the solution of transport equation in unstructured meshes and, therefore, for realistic application to reactor analysis [3, 4, 5]. However, since reactor transport problems are often characterised by collision-dominated regimes, any iterative solution of the transport equation - including MOC - generally requires a great number of iterations to converge [6]. This is why the efficient use of MOC needs acceleration techniques. The main idea of a multi-grid approach to speed up the convergence of transport iterations is to build a hierarchy of low-order problems, each solved in a more coarsely discretised phase space and consequently involving fewer unknowns. The solution of a given low-order problem provides a correction to accelerate the flux moments resulting from the previous iteration on the immediately higher level.

In this paper, a new non-linear space-angle multi-grid acceleration method dealing with full anisotropy of scattering is proposed. We extend and generalise some previous results for a spatial multi-grid method [7]. To illustrate our acceleration, we focus upon a two-level scheme. This choice is not restrictive, as the algorithm can be extended to any number of levels with no significant complications. The first step is to define a more coarsely discretised phase space. Coarsening affects both spatial and angular variable. For the spatial variable we act as follows. From the MOC spatial discretisation, that we will henceforth call fine grid, an associated coarse grid is obtained from the previous via a simple agglomeration procedure (see Fig. 1), in which each coarse mesh \mathcal{D}_I is obtained by fusing together adjacent fine meshes. Consequently, the measure of each macro-region is given by the sum of the measures of all the fine regions in it:

$$\mathcal{D}_I = \bigcup_{i \in I} \mathcal{D}_i \quad \Rightarrow \quad V_I = \sum_{i \in I} V_i . \quad (1)$$

This requires a table of correspondences between the two spatial grids, and the implementation of a homogenisation technique in order to derive the material properties for the coarse meshes (typically the cross sections). In our case, the coarse-mesh total cross sections are obtained from a flux-volume homogenisation procedure. An immediate consequence of the latter is the non-linearity of the scheme. For the angular variable, a low-order set of discrete angular directions and associated weights is employed:

$$\{\boldsymbol{\Omega}_m, \omega_m\}_{m=1, M} \text{ with } M < N. \quad (2)$$

On the coarse level, isotropic sources are used. The latter are derived from the high-order ones by an appropriate projection procedure which eliminates the angular dependence of the sources on the coarse level. Consequently, no table of correspondences between the two angular sets is needed. The scheme here presented involves a MOC-based transport sweep followed by an acceleration step consisting in iteratively solving a low-order transport problem for the zero-th flux moment. This problem is defined in order to provide, in a reference situation, the same result as the original high-order heterogeneous problem as far as averaged scalar properties are concerned. The MOC formalism is kept: outgoing angular fluxes are computed using the same propagation equation as for the fine case. However, discontinuity factors (DFs) are introduced in the balance equation in order to reconstruct outgoing and incoming currents on each macro-region. Finally, a prolongation operator, using shape factors depending on the fine flux, is employed to reconstruct the flux moments on the fine grid. This method was initially meant to speed up convergence of inner iterations. Afterwards, it has been extended to the acceleration of outer iterations. Both applications are presented here.

The paper is structured as follows: in section 2 the basic MOC equations are reviewed; in section 3 we give the operators of restriction and prolongation, and discuss the introduction of DFs; the low-order operator is introduced in section 4, where a complete discussion of the equations is given; in section 5 we present the application of our acceleration scheme to outer iterations; tests are given in section 6 for eigenvalue problems for a realistic BWR assembly and for the C5G7MOX Benchmark; closing conclusions are presented in the last section.

2 Method of Characteristics

The basis for reactor core, assembly-level transport calculations is the one-group linear Boltzmann equation. The most straightforward method to iteratively solve it is the source iteration (SI) which

computes updated angular fluxes assuming that the emission density is known:

$$\begin{cases} (\boldsymbol{\Omega} \cdot \nabla + \sigma) \psi^{(n+1)}(x) = q^{(n)}(x) & x \in X, \\ \psi^{(n+1)}(x) = \psi_{-}^{(n)}(x) & x \in \partial_{-} X. \end{cases} \quad (3)$$

In this equation, n denotes the iteration index, $X = \{x : \mathbf{r} \in \mathcal{D}, \boldsymbol{\Omega} \in 4\pi\}$ is the phase space with its boundary $\partial_{-} X$, and σ is the total cross section. The emission density reads as follows:

$$q = H\psi + S \quad (4)$$

where S stands for the external source (including fission contributions and transfers from the other groups), and

$$(H\psi)(x) = \sum_k^K \sigma_{s_k}(\mathbf{r}) \sum_{l \leq |k|} A_{kl}(\boldsymbol{\Omega}) \phi^{kl}(\mathbf{r}) \quad (5)$$

is the within-group-scattering term, written using the classical expansion of the collision term on spherical harmonics $A_{kl}(\boldsymbol{\Omega})$.

In this section we briefly review the basics of the method of the characteristics for unstructured meshes. More details about the angular and spatial approximations as well as the derivation of the equations can be found in [3, 8].

2.1 Approximations

The method is based upon two main spatial approximations. First a flat-source approximation is made on each region:

$$q(\mathbf{r}, \boldsymbol{\Omega}) = \sum_i \chi_i(\mathbf{r}) q_i(\boldsymbol{\Omega}), \quad (6)$$

where $\chi_i(\mathbf{r})$ is the characteristic function of region i . Further, the angular flux is assumed to be constant across sectional area associated to each trajectory

$$\psi(r, \boldsymbol{\Omega}) = \sum_{t|\boldsymbol{\Omega}} \chi_t(\mathbf{r}_{\perp}) \psi_t(z, \boldsymbol{\Omega}), \quad (7)$$

where $\chi_t(\mathbf{r}_{\perp})$ is the characteristic function associated to the cross sectional area of trajectory t , z is the coordinate along the trajectory, and $\psi_t(z, \boldsymbol{\Omega})$ is the angular flux along the trajectory.

The phase space in which the discretised transport problem is to be solved is defined as

$$X = \{\mathcal{D}_i\} \times \{\Omega_n\} . \quad (8)$$

2.2 Basic Equations

MOC balance and propagation equations are obtained by a projective technique involving Eq. (3) and its integral form. The propagation equation is given by the integral transport equation across a region i and along a trajectory t parallel to the discrete direction Ω_n :

$$\psi_{+,i}(t, \Omega_n) = \psi_{-,i}(t, \Omega_n) + \beta_i(t, \Omega_n) [q_i(\Omega_n) - \sigma_i \psi_{-,i}(t, \Omega_n)] , \quad (9)$$

where the escape coefficient is

$$\beta_i(t, \Omega_n) = \frac{1 - e^{-\sigma_i R_i(t, \Omega_n)}}{\sigma_i} , \quad (10)$$

and $R_i(t, \Omega_n)$ is the length of the trajectory within the region. The average emission density $q_i(\Omega_n)$ is written as:

$$q_i(\Omega_n) = C_i(\Omega_n) + S_i(\Omega_n) , \quad (11)$$

where $S_i(\Omega_n)$ is the average external source and $C_i(\Omega_n)$ is the within-group transfer. The latter is given by:

$$C_i(\Omega_n) = \sum_{k=0}^{K_i} \sigma_{s_k, i} \sum_{l \leq |k|} A^{kl}(\Omega_n) \phi_i^{kl} , \quad (12)$$

where K_i is the degree of anisotropy in region i . The moments ϕ_i^{kl} of the angular flux are obtained as follows:

$$\phi_i^{kl} = \sum_n w_n A^{kl}(\Omega_n) \psi_i(\Omega_n) . \quad (13)$$

The balance equation is obtained by integration of Eq. (3) over the volume of a region i :

$$\sum_{t \parallel \Omega_n, t \cap i} w_{\perp}(t, \Omega_n) [\psi_{+,i}(t, \Omega_n) - \psi_{-,i}(t, \Omega_n)] + \sigma_i \psi_i(\Omega_n) V_i = q_i(\Omega_n) V_i , \quad (14)$$

the sum in t being done for all trajectories with direction Ω_n that intersect region i , and the weight $w_{\perp}(t)$ represents the orthogonal area associated with the trajectory.

2.3 Boundary Conditions

We consider two kinds of boundary conditions that are used for numerical solutions of the transport equation in the TDT solver:

- geometrical motions (e.g. translation, rotation or planar symmetry) are used to reduce the size of a domain that has these symmetries. They may be thought as "exact" boundary conditions. For this case, a special set of periodic trajectories, often called *cyclic* trajectories is used.
- albedo conditions introduce a physical approximation to represent the spatial and angular distribution of the particles re-entering the geometrical domain \mathcal{D} .

For the albedo cases, the general approach in TDT is the following. The boundary $\partial\mathcal{D}$ is decomposed into a set of surfaces $\{\alpha\}$ and the entering and exiting angular domains $\{2\pi\}_\pm$ into a set of angular subdomains $\{\rho\}_\pm$. The current of particles leaving (-) each surface α through angular domain ρ is evaluated. In the iterative scheme, the latter is used to compute the entering (+) current with the help of an albedo condition:

$$J_{\alpha,+}^\rho \underset{\text{albedo}}{\Rightarrow} J_{\alpha,-}^\rho . \quad (15)$$

For a trajectory t entering through surface α with angular direction $\mathbf{\Omega} \in \rho$, the incoming flux is given by:

$$\psi_-(t, \mathbf{\Omega}) = \frac{1}{c_\alpha^\rho} J_{\alpha,-}^\rho , \quad (16)$$

where

$$c_\alpha^\rho = \int_\alpha dS \int_\rho d\Omega |\mathbf{\Omega} \cdot \mathbf{n}| . \quad (17)$$

In the following part of the paper, we will consider only isotropic albedo cases. In this case we have:

$$\psi_-(t, \mathbf{\Omega}) = \frac{1}{c_\alpha} J_{\alpha,-} , \quad (18)$$

with

$$c_\alpha = \int_\alpha dS \int_{2\pi+} d\Omega |\mathbf{\Omega} \cdot \mathbf{n}| = \sum_n \omega_n \sum_{t|\mathbf{\Omega}_n, t \cap \alpha} w_\perp(t, \mathbf{\Omega}_n) . \quad (19)$$

3 General Framework

In this section we present the prolongation and restriction procedures and discuss the introduction of the discontinuity factors.

3.1 Prolongation and Restriction

In classical linear multi-grid methods [9, 10], the low-order problem is commonly solved for an additive error to the high-order calculation. Here, instead, the acceleration step consists in solving a simplified transport problem providing a scalar flux $\{\phi_I^h\}$ on the coarse level. This flux is directly used to reconstruct the fine angular moments resulting from the previous transport iteration ($n + 1$). The fine moments are consequently accelerated as follows:

$$(\phi_i^{kl})_{acc}^{(n+1)} = (\gamma_i^{kl})^{(n+1)} (\phi_I^h)^{(\infty)}, \quad \forall i \in I. \quad (20)$$

To do this, we employ shape factors $\{\gamma_i^{kl}\}$ depending on the unaccelerated flux. They are defined as:

$$\gamma_i^{kl} = \frac{\phi_i^{kl}}{\bar{\phi}_I}, \quad (21)$$

where $\bar{\phi}_I$ is the volume-averaged scalar flux:

$$\bar{\phi}_I = \frac{1}{V_I} \sum_{i \in I} \phi_i V_i. \quad (22)$$

The prolongation procedure (21) is equivalent to applying a multiplicative correction to the high-order calculation [11]. We note that, in a reference situation where the converged fine flux is available, the solution of the low-order problem must preserve the integral of the scalar flux on each mesh of the coarse spatial grid, i.e.

$$\phi_I^h = \bar{\phi}_I. \quad (23)$$

This requirement is fundamental for the scheme to converge. Indeed, our choice for homogenisation and the introduction of the DFs are strictly tied to the fulfilment of this condition.

On the coarse level, isotropic sources are used. They are obtained from the high-order ones by a space-angle restriction procedure. The latter is applied whether to the emission density q_i when computing the DFs, or to the external source S_i when solving the low-order problem. Let be u_i one of the above-mentioned sources, we have:

$$\bar{u}_I = \frac{1}{4\pi} \sum_n \omega_n \sum_{i \in I} u_i(\Omega_n) V_i. \quad (24)$$

For the spatial variable, this projection consists in volume-averaging on each mesh of the coarse grid.

Further, the integration over all directions eliminates the angular dependence on the coarse level. This permits to avoid building a table of correspondences between the two angular grids. We note that, by construction, the scalar source are preserved on both levels.

3.2 Homogenisation

This part has been inspired by Koebke's earlier works [12, 13] on homogenisation. The main idea is that an equivalent homogenised problem can be built for a given heterogeneous problem by introducing additional degrees of freedom such as discontinuity factors. Koebke's method dealt with a nodal approximation of the transport equation, and discontinuity factors were applied to the interface scalar fluxes in order to fulfil the so-called equivalence theorem. Following an approach analogous to Koebke's, we explain why the DFs have been introduced into our acceleration, and how this permits to respect condition (23).

The availability of an accurate heterogeneous solution of Eq. (3) is assumed in the following discussion. The heterogeneous solution satisfies the integral neutron balance equation on whatever coarse mesh \mathcal{D}_I :

$$\int_{\partial\mathcal{D}_I} \mathbf{J}(\mathbf{r}) \cdot d\mathbf{S} + \int_{\mathcal{D}_I} \sigma(\mathbf{r}) \phi(\mathbf{r}) d\mathbf{r} = \int_{\mathcal{D}_I} Q(\mathbf{r}) d\mathbf{r} . \quad (25)$$

We write an analogous equation for the homogenised low-order problem:

$$\int_{\partial\mathcal{D}_I} \mathbf{J}^h(\mathbf{r}) \cdot d\mathbf{S} + \int_{\mathcal{D}_I} \sigma^h(\mathbf{r}) \phi^h(\mathbf{r}) d\mathbf{r} = \int_{\mathcal{D}_I} Q^h(\mathbf{r}) d\mathbf{r} . \quad (26)$$

Let the scalar source Q^h be defined as the volume-averaged fine one. The homogenised total cross section is taken piece-wise constant:

$$\sigma^h(\mathbf{r}) = \sum_I \chi_I(\mathbf{r}) \sigma_I^h . \quad (27)$$

If the leakage term is preserved, we are able to ensure the preservation of the total reaction rate as well, for any arbitrary value of the homogenised total cross sections σ^h . Thus, we are allowed to choose a flux-volume weighting procedure:

$$\sigma_I^h = \frac{\int_{\mathcal{D}_I} \sigma \phi d\mathbf{r}}{\int_{\mathcal{D}_I} \phi d\mathbf{r}} , \quad (28)$$

which yields the preservation of the integral of the scalar flux and, therefore the fulfilment of condition (23). However, once homogenised total cross sections are chosen as in Eq. (28), additional degrees

of freedom are necessary to preserve the leakage term. Some approaches can be found in literature. As an example, one can consider the coarse mesh finite difference (CMFD) method [11, 14] that acts as follows: the leakage is expressed in terms of the net currents on each surface of a rectangular homogenised region, diffusion is used as a low-order operator and coupling correction coefficients on each surface are introduced in order to match the average net currents. The novelty in this work is that a transport-like operator is employed for the homogenised problem. Furthermore, we decided to write the leakage in terms of the outgoing (+) and the incoming (-) currents as follows:

$$\int_{\partial\mathcal{D}_I} \mathbf{J}(\mathbf{r}) \cdot d\mathbf{S} = J_{+,I} - J_{-,I} , \quad (29)$$

and to ensure the preservation of each one of them. We indicate with $\{\hat{J}_{\pm,I}\}$ the currents given by the low-order transport operator and with $\{J_{\pm,I}^h\}$ the corrected ones. A discontinuity factor is defined for each one of them, in order to ensure the following:

$$J_{\pm,I} = J_{\pm,I}^h = f_{\pm,I} \cdot \hat{J}_{\pm,I} . \quad (30)$$

The discontinuity factors $\{f_{\pm,I}\}$ are calculated as the ratio between a reference value and the value produced by the low-order operator in a reference situation.

Summarising, the introduction of the DFs as additional degrees of freedom permits to define an equivalent low-order problem which is able to reproduce the same result as for the reference heterogeneous problem when considering averaged properties. However, the problem in practical applications is that these factors, as the diffusion-like coupling coefficients for the CMFD formulation, should be computed a priori, since we do not have access to the converged fine flux before the iterative procedure is achieved. This is why a dynamic calculation of the DFs is performed: DFs are computed after each fine iteration, taking the latter as a reference situation.

3.3 V-cycle scheme

Our two-level method can be well described as a V-cycle. A general sketch is given in Fig. 2. After each fine transport iteration, an associated low-order problem is iteratively solved on the coarse grid, using the homogenised parameters derived from the previous transport sweep on the fine level. A maximum number M_n of iterations may be fixed a priori. The coarse solution is used to reconstruct the fine flux moments with the help of the shape factors. Then, the source is updated for the next transport sweep.

4 Acceleration of Inner Iterations

At each transport sweep, the region-averaged angular fluxes are computed in terms of sources and boundary conditions:

$$\psi_{-}^{(n)}(t, \mathbf{\Omega}), q_i^{(n)}(\mathbf{\Omega}) \rightarrow \psi_i^{(n+1)}(\mathbf{\Omega}) . \quad (31)$$

Then, an associated low-order problem is solved in order to speed up the convergence of the inner iterations. In this section we point out the main aspects of our acceleration. The low-order problem and its iterative solution are discussed.

4.1 Low-Order Problem

On the homogenised coarse grid, we consider a transport problem analogous to the fine case. The MOC-formalism is used to iteratively solve it. Let be p the iteration index, we have:

$$\begin{cases} (\nabla \cdot \mathbf{\Omega} + \sigma^h) \hat{\psi}^{(p+1)} = q^{h,(p)} & \text{in } X' \\ \hat{\psi}^{(p+1)} = \hat{\psi}_{-}^{(p)} & \text{on } \partial_{-} X' . \end{cases} \quad (32)$$

In this equation q^h is the coarse emission density and σ^h is the homogenised total cross section obtained as:

$$\sigma_I^h = \frac{1}{V_I} \sum_{i \in I} \sigma_i \gamma_i^{(n+1)} V_i , \quad (33)$$

where γ_i is the shape factor for the scalar flux as in Eq. (21). The more coarsely discretised phase space is written as $X' = \{\mathcal{D}_I\} \times \{\mathbf{\Omega}_m\}$.

As earlier mentioned, because of homogenisation and source projection, the currents computed by the low-order transport operator are not consistent with those resulting from the high-order calculation. In particular, in a reference situation where the converged flux is available, the leakage term is not preserved on the two levels. Thus, we cannot directly employ $\hat{\psi}$ to compute the scalar flux needed for prolongation in Eq. (20). Nevertheless, this drawback can be overcome by modifying the iterative approach for the low-order problem. Unlike for the fine level, each iteration is performed to compute the global incoming and outgoing currents per macro, without evaluating region-averaged angular fluxes. The same sweep philosophy is used. Continuity of the interface angular fluxes along each trajectory is still valid. Afterwards, the scalar flux $\{\phi_I^h\}$ is computed in a post-treatment phase involving the discontinuity factors previously computed.

The same spatial approximations as for the fine level are made. Thus, the source is assumed to be flat on each homogenised mesh:

$$q^h(\mathbf{r}, \boldsymbol{\Omega}) = \sum_I \chi_I(\mathbf{r}) q_I^h(\boldsymbol{\Omega}) , \quad (34)$$

where $\chi_I(\mathbf{r})$ is the characteristic function of region I . Further, we make the assumption that the angular flux is constant across sectional area associated to each trajectory as in Eq. (14):

$$\hat{\psi}(r, \boldsymbol{\Omega}) = \sum_{t \parallel \boldsymbol{\Omega}} \chi_t(\mathbf{r}_\perp) \hat{\psi}_t(z, \boldsymbol{\Omega}) . \quad (35)$$

4.2 Equations

A MOC-like formalism is kept on the coarse grid. Indeed, like for the fine case, two main equations are employed: a propagation equation giving the outgoing (+) angular flux along each trajectory in terms of the incoming (-) angular flux and the internal source, and a balance equation for the scalar flux. The propagation equation is obtained by the integral transport equation across a macro-region I and along a trajectory t parallel to the discrete direction $\boldsymbol{\Omega}_m$:

$$\hat{\psi}_{+,I}(t, \boldsymbol{\Omega}_m) = \hat{\psi}_{-,I}(t, \boldsymbol{\Omega}_m) + \beta_I^h(t, \boldsymbol{\Omega}_m) \left[q_I^h - \sigma_I^h \hat{\psi}_{-,I}(t, \boldsymbol{\Omega}_m) \right] . \quad (36)$$

The escape coefficient is defined in an analogous way to the fine case:

$$\beta_I^h(t, \boldsymbol{\Omega}_m) = \frac{1 - e^{-\sigma_I^h R_I(t, \boldsymbol{\Omega}_m)}}{\sigma_I^h} , \quad (37)$$

where σ_I^h is the homogenised total cross section defined in Eq. (33), and $R_I(t, \boldsymbol{\Omega}_m)$ is the length of the chord intersected in the macro-region I by the trajectory t . By analogy to the fine level, the coarse emission density q_I^h is written in terms of an external source \bar{S}_I , which is obtained by restriction (24), and a collision term C_I^h :

$$q_I^h = C_I^h + \bar{S}_I . \quad (38)$$

We will come back later to the collision term. Total outgoing and incoming currents are built up at each coarse iteration as follows:

$$\hat{J}_{\pm, I} = \sum_m \omega_m \sum_{t \parallel \boldsymbol{\Omega}_m} \omega_\perp(t) \hat{\psi}_{\pm, I}(t, \boldsymbol{\Omega}_m) . \quad (39)$$

These currents are corrected with the help of the discontinuity factors, and then used in the balance equation giving the coarse scalar flux:

$$f_{+,I} \cdot \hat{J}_{+,I} - f_{-,I} \cdot \hat{J}_{-,I} + \sigma_I^h \phi_I^h V_I = Q_I^h V_I , \quad (40)$$

where the scalar source Q_I^h is obtained by integration of the emission density q_I^h over all directions as follows:

$$Q_I^h = \sum_m \omega_m q_I^h . \quad (41)$$

It remains to explain how the collision term is defined and how the emission density is updated.

4.3 Collision Term

As already mentioned, the low-order problem is defined in a reference situation where the fine converged flux is used and the source on the coarse level is obtained by projection:

$$q_I^h = \bar{q}_I . \quad (42)$$

Now, in our iterative scheme, the coarse emission density is written in terms of the within-group scattering contribution and the external source as in Eq. (38). This means that, in the above-mentioned reference situation, further iterations must not modify the value of the coarse scalar flux in order not to compromise the convergence of the scheme, which entails:

$$C_I^h = \bar{C}_I = \frac{1}{V_I} \sum_{i \in I} C_i V_i . \quad (43)$$

This can be achieved by choosing a flux-volume homogenisation procedure for the scattering cross sections:

$$\sigma_{s_I}^h = \frac{1}{V_I} \sum_{i \in I} \sigma_{s_{0,i}} \gamma_i V_i , \quad (44)$$

and simply defining the within-group collision term as:

$$C_I^h = \frac{1}{4\pi} \sigma_{s_I}^h \phi_I^h V_I . \quad (45)$$

As a consequence, the coarse emission density is iteratively updated as follows:

$$q_I^{h,(p)} = \frac{1}{4\pi} \sigma_{s_I}^h \phi_I^{h,(p)} + \bar{S}_I, \quad (46)$$

where p is the iteration index for the coarse level calculation.

4.4 Boundary Conditions

Like for the fine case, two kinds of boundary conditions have been considered: geometrical motions using cyclic trajectories, and isotropic albedo conditions.

In the case of geometrical motions, the same approach as for the traditional MOC [8] is kept. Therefore, the angular flux $\hat{\psi}(x)$ along a periodic compound trajectory requires the simultaneous computation of the two angular flux defined by a unit incoming angular flux in the absence of volumetric sources, $\hat{\psi}_{bd}(x)$, and by the volumetric sources with zero incoming angular flux, $\hat{\psi}_q(x)$. Once these two fluxes have been computed, the final angular flux is given by:

$$\hat{\psi}(x) = \frac{\hat{\psi}_q(x)}{1 - \hat{\psi}_{bd}(x)} \hat{\psi}_{bd}(x) + \hat{\psi}_q(x). \quad (47)$$

In the albedo condition case, the boundary is decomposed into a set of surfaces $\{\beta\}$, and table of correspondences is established between the fine and the coarse surfaces. In particular we have:

$$S_\beta = \sum_{\alpha \in \beta} S_\alpha. \quad (48)$$

By analogy with the fine level, the incoming flux associated to a trajectory t entering through surface β with angular direction $\mathbf{\Omega}_m$ is given by:

$$\hat{\psi}_-(t, \mathbf{\Omega}_m) = \frac{1}{c_\beta} J_{\beta,-}^h, \quad (49)$$

where

$$c_\beta = \int_\beta dS \int_{2\pi+} d\Omega |\mathbf{\Omega} \cdot \mathbf{n}| = \sum_m \omega_m \sum_{t \in \mathbf{\Omega}_m, t \cap \beta} w_\perp(t, \mathbf{\Omega}_m). \quad (50)$$

For the first iteration we take:

$$J_{\beta,-}^{h,(0)} = \frac{1}{S_\beta} \sum_{\alpha \in \beta} S_\alpha J_{\alpha,-}^{(n+1)}, \quad (51)$$

then, the incoming currents through each macro surface β are updated with an albedo condition derived

from the fine level:

$$J_{\beta,+}^h \xrightarrow{\text{albedo}} J_{\beta,-}^h . \quad (52)$$

4.5 Computing DFs

Here we focus upon the leakage term. We discuss how discontinuity factors (DFs) are computed in the implementation of our scheme. Their evaluation is situated between a fine iteration and the solution of the associated low-order problem. After a transport sweep, the incoming (-) and the outgoing (+) currents on each coarse-mesh \mathcal{D}_I are available:

$$J_{\pm,I}^{(n+1)} = \sum_n w_n \sum_{t \cap \Omega_n, t \cap I} w_{\perp}(t) \psi_{\pm, i \in \partial I}^{(n+1)}(t, \Omega_n) , \quad (53)$$

where $\psi_{\pm, i \in \partial I}^{(n+1)}$ is the angular flux entering (-) or leaving (+) a portion of a fine region's boundary $\partial \mathcal{D}_i$ having a non-null intersection with the boundary $\partial \mathcal{D}_I$ of the coarse region \mathcal{D}_I . It is worth noting that, in practice, a modification of the implementation of the fine transport iterations in TDT code is needed to compute these currents. More details about this point can be found in appendix A. We remind the reader that, when defining DFs, we want to preserve the leakage term on each coarse-mesh \mathcal{D}_I for a reference situation. In this work, we chose to achieve it by preserving the total incoming and outgoing currents. The reference is given by the currents at iteration $(n+1)$ obtained from the emission density and the boundary conditions at iteration (n) . Consequently, we consider the following fixed-source problem:

$$\begin{cases} (\boldsymbol{\Omega} \cdot \nabla + \sigma^h) \hat{\psi} = \bar{q} & \text{on } X' \\ \hat{\psi} = \hat{\psi}_- & \text{on } \partial_- X' \end{cases} \quad (54)$$

where the source is given by projecting $\{q_i^{(n)}\}$ as in Eq. (24) and the incoming flux is obtained as shown in subsection 4.4 using $\{J_{\alpha,-}^{(n)}\}$. The total cross section is given by Eq. (33), and the more coarsely discretised phase space X' is the same as in Eq. (32). Within the MOC framework, only one sweep is needed to solve Eq. (54). Starting from the boundary of the domain the angular flux leaving a macro-region \mathcal{D}_I is computed for a characteristic trajectory t via Eq. (36), in which \bar{q}_I is used. The outgoing flux is used as incoming flux for the following region along the above-mentioned trajectory. The total incoming (-) and outgoing currents (+) are given by Eq. (39). Then, the DFs are given as the ratio

between the heterogeneous and the homogeneous currents as follows:

$$f_{\pm,I} = \frac{J_{\pm,I}}{\hat{J}_{\pm,I}} \Big|_{ref} . \quad (55)$$

These coefficients are taken as constant in the low-order calculation and, after each coarse iteration, the incoming and outgoing currents are corrected as follows:

$$J_{\pm,I}^{h,(p)} = f_{\pm,I} \cdot \hat{J}_{\pm,I}^{(p)} , \quad (56)$$

where p is the iteration index.

4.6 Note on Albedo Conditions - Boundary DFs

As above mentioned, on the coarse level the boundary is decomposed into a coarser set of surfaces $\{\beta\}$. The outgoing current through each surface α is reconstructed and updated as follows:

$$(J_{\alpha,+})_{acc}^{(n+1)} = \zeta_{\alpha}^{(n+1)} (J_{\beta,+}^h)^{(\infty)} , \quad \forall \alpha \in \beta . \quad (57)$$

The shape factors $\{\zeta_{\alpha}\}$ are defined using the unaccelerated leaving currents as:

$$\zeta_{\alpha} = \frac{J_{\alpha,+}}{\bar{J}_{\beta,+}} , \quad (58)$$

where $\bar{J}_{\beta,+}$ is the average current on the macro surface β :

$$\bar{J}_{\beta,+} = \frac{1}{S_{\beta}} \sum_{\alpha \in \beta} S_{\alpha} J_{\alpha,+} . \quad (59)$$

We note that if the converged fine flux is available, the partial currents through surfaces β must be preserved on both levels, i.e. the following condition must be fulfilled:

$$J_{\beta,+}^h = \bar{J}_{\beta,+} . \quad (60)$$

Now, the introduction of DFs ensures the preservation of the global incoming and outgoing currents on each region of the coarse discretisation. However, this does not entail that the current of particles leaving the boundary of the domain is preserved as well. Boundary discontinuity factors are therefore introduced

for each macro surface β and the corrected currents are given as follows:

$$J_{\beta,+}^h = f_{\beta} \hat{J}_{\beta,+} . \quad (61)$$

This permits to respect condition (60). Like for the DFs, the computation of f_{β} is performed between a transport sweep and the solution of the associated low-order problem. Reference values are represented by averaged currents at the fine iteration $(n + 1)$ and sources at iteration (n) :

$$\psi_{-}^{(n)}(t, \boldsymbol{\Omega}), q_i^{(n)}(\boldsymbol{\Omega}) \rightarrow \bar{J}_{\beta,+}^{(n+1)} . \quad (62)$$

After each transport fine iteration, the currents for each macro surface β are available. The low-order operator provides $\hat{J}_{\beta,+}$. Then, the boundary discontinuity factors are computed as follows:

$$f_{\beta} = \left. \frac{\bar{J}_{\beta,+}}{\hat{J}_{\beta,+}} \right|_{ref} . \quad (63)$$

These coefficients are taken as constant in the low-order calculation and, after each coarse iteration, the currents leaving the domain through surface β are corrected as follows:

$$J_{\beta,+}^{h,(p)} = f_{\beta} \hat{J}_{\beta,+}^{(p)} , \quad (64)$$

where p is the iteration index for the coarse-level calculation.

5 Acceleration of Outer Iterations

In the previous part of our work, we focused upon the one-group problem. A spatial-angle multi-grid acceleration for the inner iterations has been presented. In this section, an extension of the low-order problem equations to the k -eigenvalue multigroup problem is proposed.

5.1 Criticality Calculations

The multi-group formulation of Boltzmann equation for multiplying systems is typically solved by the method of the power iteration [2, 15, 16] as follows:

$$F^{(p+1)}(\mathbf{r}) = \frac{1}{k_{eff}^{(p)}} A F^{(p)}(\mathbf{r}) . \quad (65)$$

In this equation $F(\mathbf{r})$ is the spatial distribution of fission neutrons produced in the reactor:

$$F(\mathbf{r}) = \sum_{g'} (\nu\sigma_f)^{g'}(\mathbf{r}) \phi_{g'}(\mathbf{r}) , \quad (66)$$

and A is the scalar multi-group transport operator. Power iteration is often referred to as outer iteration.

In TDT code, the eigenvalue is updated as follows:

$$k_{eff}^{(p+1)} = k_{eff}^{(p)} \frac{\int_{\mathcal{D}} F^{(p+1)}(\mathbf{r}) d\mathbf{r}}{\int_{\mathcal{D}} F^{(p)}(\mathbf{r}) d\mathbf{r}} . \quad (67)$$

Each power iteration requires the iterative solution of a fixed-source multi-group upscattering problem for the angular flux. Let be l the iteration index, we have:

$$L^g \psi_g^{(l+1)} = H^{g \rightarrow g} \psi_g^{(l+1)} + \sum_{g' < g} H^{g' \rightarrow g} \psi_{g'}^{(l+1)} + \sum_{g' > g} H^{g' \rightarrow g} \psi_{g'}^{(l)} + \frac{1}{4\pi} Q_f^g , \quad (68)$$

In this equation, $L^g \doteq \mathbf{\Omega} \cdot \nabla + \sigma^g$ is the one-group transport operator, while $H^{g' \rightarrow g}$ is the slowing-down operator from group g' to group g , and Q_f^g is the fission source for group g . This problem is solved using a Gauß-Seidel iterative procedure. If no up-scattering is present, which is the case for fast groups, only one iteration is needed. Neglecting the iteration index, on each region Eq. (68) reads:

$$J_{+,i}^g(\mathbf{\Omega}_n) - J_{-,i}^g(\mathbf{\Omega}_n) + \sigma_i^g \psi_i^g(\mathbf{\Omega}_n) V_i = C_i^g(\mathbf{\Omega}_n) V_i + \sum_{g' \neq g} C_i^{g' \rightarrow g}(\mathbf{\Omega}_n) V_i + \frac{1}{4\pi} Q_{f,i}^g V_i , \quad (69)$$

where $C_i^{g' \rightarrow g}$ is the group-to-group collision contribution which is written as follows:

$$C_i^{g' \rightarrow g}(\mathbf{\Omega}_n) = \sum_k \sigma_{sk,i}^{g' \rightarrow g} \sum_{l < |k|} A_{kl}(\mathbf{\Omega}_n) \phi_i^{kl,g'} , \quad (70)$$

and the fission source per group $Q_{f,i}^g$ is written as:

$$Q_{f,i}^g = \frac{1}{k_{eff}} \sum_{x \in i} \chi_x^g F_{i,x} , \quad (71)$$

the sum being done over all the isotopes in i . The fission source $F_{i,x}$ for an isotope x in a mesh i is defined as follows:

$$F_{i,x} = \sum_{g'} (\nu\sigma_f)_x^{g'} \phi_i^{g'} . \quad (72)$$

5.2 Extension of the Low-Order Equations

The basic idea is to exploit the coarse scalar fluxes computed while accelerating inner iterations, before performing a new power iteration on the fine level. To do this, after each fine outer iteration, we define an associated low-order eigenvalue multi-group problem on the coarse level. The solution of this problem $\{\phi_I^{h,g}\}$ is then used, together with the previously computed shape factors per group $\{\gamma_i^{kl,g}\}$, to reconstruct the flux moments on the fine level:

$$\left(\phi_i^{kl,g}\right)_{acc} = \gamma_i^{kl,g} \phi_I^{h,g}, \quad \forall i \in I . \quad (73)$$

The so-obtained scalar flux is used to correct the fission source:

$$(F_{x,i})_{acc} = \sum_{g'} (\nu\sigma_f)_x^{g'} \left(\phi_i^{g'}\right)_{acc} , \quad (74)$$

and consequently to accelerate the multiplication eigenvalue. The low-order problem must be defined so that, in a reference situation where the converged fine solution is available, the scalar balance equation per macro-region \mathcal{D}_I and per group g is respected on both levels. On the coarse level, the balance equation reads:

$$f_{+,I}^g \cdot \hat{J}_{+,I}^g - f_{-,I}^g \cdot \hat{J}_{-,I}^g + \sigma_I^{h,g} \phi_I^{h,g} V_I = Q_I^{h,g} V_I . \quad (75)$$

The DFs $\{f_{\pm,I}^g\}$ come from the previous fine outer iteration, as well as the homogenised total cross sections. The source $Q_I^{h,g}$ is obtained by integrating the coarse isotropic emission density $q_I^{h,g}$ over all directions $\{\Omega_m\}$. The latter term is written as:

$$q_I^{h,g} = C_I^{h,g} + \sum_{g' < g} C_I^{h,g' \rightarrow g} + \sum_{g' > g} C_I^{h,g' \rightarrow g} + \frac{1}{4\pi} Q_{f,I}^{h,g} , \quad (76)$$

respectively in terms of the within-group, the down-scattering, the up-scattering terms and the fission source per group g . By analogy with the within-group case, the group-to-group collision term is written as:

$$C_I^{g' \rightarrow g, h} = \frac{1}{4\pi} \sigma_{sI}^{g' \rightarrow g, h} \phi_I^{g', h} V_I , \quad (77)$$

with

$$\sigma_{s_I}^{g' \rightarrow g, h} = \frac{1}{V_I} \sum_{i \in I} \sigma_{s_{0,i}}^{g' \rightarrow g} \gamma_i^{g'} V_i . \quad (78)$$

On the other hand, the fission term is expressed as follows:

$$Q_I^{h,g} = \frac{1}{k_{eff}^h} \sum_{x \in I} \chi_x^g F_{x,I}^h , \quad (79)$$

where the sum is done over all isotopes x in I . The fission source is defined as:

$$F_{x,I}^h = \sum_{g'} (\nu \sigma_f)_x^{h,g'} \phi_I^{h,g'} , \quad (80)$$

with

$$(\nu \sigma_f)_x^{h,g'} = \frac{1}{V_I} \sum_{i \in I} (\nu \sigma_f)_x^{g'} \gamma_i^{g'} V_i . \quad (81)$$

Finally, k_{eff}^h is the eigenvalue of the low-order multigroup problem. This value is computed as in Eq. 65.

A particular case of this method is the acceleration of thermal iterations. This consists in solving the Eq. (68) only for thermal groups with fission source derived from the last fine outer iteration as follows:

$$Q_{f,I}^h = \bar{Q}_{f,I} = \frac{1}{V_I} \sum_{i \in I} Q_{f,i} V_i . \quad (82)$$

In this case only the thermal fluxes are reconstructed on the fine level.

6 Tests and Results

The aim of an acceleration method is to diminish, for a given class of problems, the overall computational cost, i.e. to reduce the total number of transport sweeps and the total computing time. Now, there is a trade-off between the accuracy and the computational cost of the low-order problem. An accurate approximation of the transport operator on the coarse level may drastically cut off the number of iterations but require an excessive cost in terms of computational effort and memory storage. On the other hand, a too poor approximation, which is easily solved, may not sufficiently reduce the global computational cost.

In order to test the effectiveness of our method, some tests have been performed. Results are presented in this section. All the calculations have been run on a DEC-Alpha 1000 MHz machine.

6.1 Atrium Benchmark

The case of a BWR assembly benchmark [17] is here presented. For our fine level MOC calculation, we use a 3052-region discretisation and a 6-group P1 cross sections library [18]. Because of the enforced specular boundary conditions on all sides, cyclic trajectories have been used. The trajectories have been tracked for all the directions in a product angular quadrature formula comprising 20 uniformly spaced azimuthal angles in $(0, \pi)$ and 3 polar angles derived from a Bickley-Naylor formula [19] in $(0, \pi/2)$. The tracking parameters for the fine level can be found in Table I. On the coarse level we have 136 meshes, with a ratio of fine to coarse meshes of ~ 22.4 . Two angular quadrature formulae have been considered on this level. All tracking parameters can be found in Table II. In the first row we employ the same angular set as on the fine spatial grid, which is equivalent to consider a spatial multigrid acceleration. In the second row, a low-order angular approximation is used. All the calculations have been converged to the same solution (eigenvalue $k_{eff} = 1.12854$) with a relative precision of 10^{-5} on inner iterations and eigenvalue, and a relative precision of 10^{-4} on thermal iterations and fission rates. For all the accelerated calculations, the following iterative strategy has been adopted: only one transport iteration per group is performed for each outer iteration, and the maximum number of inner and thermal iterations for the low-order problem is a priori fixed to 15 and 4 respectively. The results are shown in Tables III and IV. Those tables give global computation parameters such as the total computing time and the total number of transport sweeps. Total calculation time is divided into the different phases of the calculation: building (which includes reading geometry, tracking, and computing MOC parameters), initialisation (if present), and the solution of the k -eigenvalue multi-group problem. For the latter, the contributions from fine-level and coarse-level calculation are given between parenthesis. All the calculations are compared to the free-iteration results.

Table III refers to the case with the same set of trajectories on both levels: the number of transport sweeps is drastically reduced (ratio ~ 13.62), while the gain for the total computing time is not great (ratio ~ 3.83). In fact, the computation cost required to solve the acceleration equations is significant. Therefore, our gain in time does not show much in the overall calculation. This aspect is more evident when accelerating the thermal iterations. In this case, the further reduction of the total number of inner iterations is not followed by a consistent computing time gain. The total calculation time is greater than for the case without thermal acceleration (156.35 vs 146.30 sec). This is due to the nature of our low-order problem. In fact, since it employs a MOC-like iterative solution, its computational cost depends upon the total number of tracks. Therefore, although the number of regions on the coarse level

is significantly reduced, the ratio between the number of tracks on the fine level and those on the coarse one is only ~ 5.9 . This is why the acceleration is expensive in terms of computing time.

In Table IV we give some results for the case using a coarser tracking for the acceleration. An initialisation-like procedure has been also implemented. The initialisation consists in performing a preliminary multi-grid-accelerated transport calculation using the low-order parameters (set of angular directions and spacing between parallel trajectories) for tracking on both levels. The same above-mentioned iterative strategy is kept for the initialisation problem although this calculation is not necessarily converged to the same precision since the maximum number of outer iterations is a priori fixed to 5. The so-obtained approximated flux is then used as an initial guess. For results in Table IV, the ratio between the number of tracks on the fine level and those on the coarse one is ~ 84.46 . Consequently, the computing time for solving the acceleration equations is significantly diminished, e.g. for the non-initialised case, with thermal acceleration, it passes from 89.52 to 4.59 sec. Moreover, the use of a significantly reduced number of tracks on the coarse level permits to diminish the memory storage needs. Finally, the fastest calculation is obtained for the initialised case in which both inner and thermal iterations are accelerated.

6.2 C5G7MOX Benchmark

Here some results for the C5G7MOX Benchmark [20] are presented. We compare our results to an APOLLO2 calculation using a DP_1 acceleration [21] for the inner iterations and a synthetic acceleration for the outer iterations [22]. The MOC calculation uses a 19188-region discretisation for the geometrical domain, and the trajectories have been tracked for all the directions in a product angular quadrature formula comprising 8 uniformly spaced azimuthal angles in $(0, \pi)$ and 2 polar angles derived from a Bickley-Naylor formula in $(0, \pi/2)$. On the coarse level we employ a 1414-mesh discretisation and a low-order angular representation. All tracking parameters for both levels can be found in Table V, while results are given in Table VI. The following iterative strategy has been adopted for both methods: one transport sweep per group followed by an acceleration step for each outer iteration. Then, the acceleration for the outer iterations requires to solve a multigroup k -eigenvalue problem on the coarse level. The initialisation step consists in performing an unconverged multigrid-accelerated transport calculation by using the coarser angular representation on both levels, then we employ the solution of this problem as an initial guess. With reference to Table VI, we note that our method is slightly less effective than DP_1 for this benchmark: one more outer iteration is needed, which entails more transport sweeps (35 vs 28). On the other hand, the total computing times are comparable. It is worth noting that

the two methods have a different allocation of the total computing time. In fact, the implementation of our method does not require extra-time in the building phase, differently from the DP_N technique. However, the solution of the multigroup problem by our two-level method is more expensive (103.22 vs 37.50 sec). In this phase the most time consuming part is found to be the sweeping on the coarse level (64.34 over 103.22 sec). This is mostly due to the acceleration of the outer iterations which requires, as already mentioned, the solution of a low-order multigroup k -eigenvalue problem on the coarse level after performing an outer iteration on the fine level.

7 Conclusions and Future Work

In this work, we have presented a space-angle two-level acceleration for the MOC numerical solution of the neutron transport equation. Unlike the classical linear multi-grid methods for which a low-order problem is solved for the error at a given transport iteration, in our approach the acceleration step supplies a coarse homogenised scalar flux, which is used to reconstruct the moments of the fine angular flux. In a reference situation where the converged fine flux is available, the coarse solution must be able to reproduce the same averaged properties as the fine one. The implementation of our method has required a homogenisation/dehomogenisation technique, which has led us to the main approximations of our scheme: the discontinuity factors and the shape factors. Some parallels and distinctions with the CMFD approach proposed in literature have been drawn. Furthermore, we note that, since our method uses a MOC-like formalism to solve the low-order problem, no constraints stand against the fact of considering an unstructured grid on the coarse level. This is a clear advantage with respect to CMFD or other non-linear diffusion-like acceleration techniques which generally require to superimpose a rectangular acceleration mesh on the heterogeneous geometry. This aspect makes our method attractive, for example, to whole core transport calculations. For the latter, an accurate geometrical description of elements close to the boundary (e.g. baffle/reflector representation) requires indeed an unstructured grid. Finally, a transport-like operator is employed on the coarse level, the correction provided by our acceleration step can be more accurate than that provided by CMFD for a class of reactor transport problems in which diffusion modes are not dominant and transport effects due to higher modes become more important (e.g. accident situations).

Tests performed for the Atrium assembly have given encouraging results. They showed that our approach may be very effective in cutting off the number of transport sweeps. However, the solution of the acceleration problem may be too expensive if using the same set of trajectories on both fine and coarse

levels. This is because the acceleration step is still based upon a MOC-like approach and, consequently, its cost depends on the number of tracks (i.e. the total number of intersections of trajectories with regions where the number of trajectories depends upon the angular quadrature formula and the spacing between the trajectories). Then a space-angle method, making use of a low-order tracking, permits to significantly reduce the computing time and the memory storage needs for acceleration. Nevertheless, as a general consideration, we note that this further approximation of the transport operator on the coarse level may lightly worsen the total number of transport sweeps.

Furthermore, tests performed for the C5G7MOX benchmark showed that our method can perform well for reactor transport problems. It does not need extra work in the building phase, which is a clear advantage. However, the computational effort for solving the acceleration equations still remains high for such a case. The aim of this paper was to introduce a new method and show that it can be effective for a class of transport problems. Further work is needed for improving and optimisation.

Work is under way to investigate the extension of the method to more levels for reactor-core-size transport problems. We note that the use of more grids will not further diminish the number of transport sweeps, but only the computational effort needed for the acceleration phase. In this case, one can imagine to employ, on the first coarse level, an accurate approximation of the transport operator and the phase space in order to drastically cut off the number of iterations, and use more coarsely defined problems on the lower levels in order to reduce the computation time.

A Modifying MOC on the Fine Grid

Within the general framework of MOC, the tracking is built by computing and storing a set of geometrical data. In practical applications, a record is created for each trajectory:

$$\{r_i, l_i \mid i = 1, M\} , \quad (83)$$

where M is the number of intersections with regions; and r_i, l_i are the order number of region i and the track length of the trajectory across this region, respectively. Therefore, sweeping a trajectory consists in covering, in the order given by record (83), the M chords given by intersection of the trajectory with the fine regions. This approach has been kept to solve the low order problem, with the creation of an analogous record for each trajectory:

$$\{r_I, l_I \mid I = 1, M'\} , \quad (84)$$

where M' is the number of intersections with macro regions; and r_I, l_I are the order number of region I and the track length of the trajectory across this region, respectively.

In the implementation of MOC, one free iteration consists in computing the average angular flux ψ_i on each region D_i and, if needed, the currents leaving the domain through the discretised boundary α . However, in our scheme, global incoming and outgoing currents on each macro region $J_{\pm, I}$ have to be evaluated in order to compute DFs with Eqs. (53) and (55). In practice, the aim is to know when the boundary of a coarse mesh is crossed. This means that the fine discretisation has to *know* the coarse one, and that the tracking on the fine grid has to be reformulated to take into account both grids and the table of correspondence between them. To do this, we have introduced two more records for the trajectory on the fine grid:

- a coarse record giving, for each macro region I crossed by the trajectory, its order number:

$$\{r_I \mid I = 1, M'\} , \quad (85)$$

- a record giving, for each of these macro-regions, the number of fine regions in it:

$$\{n_I \mid I = 1, M'\} . \quad (86)$$

Consequently, the sweeping of a trajectory on the fine grid is modified. In fact, instead of a single cycle

over the M fine chords, a double cycle is performed: a cycle over the M' coarse chords, and for each one of them an inner cycle over all the fine chords in it. This allows us to know when the boundary of a coarse mesh is crossed, and to compute the currents we are interested in. Note that, if the same set of trajectories is employed on both grids, record (85) is derived directly from record (84).

Acknowledgement

The author would like to thank R. Sanchez and S. Santandrea for helpful discussions and suggestions during the preparation of this paper.

References

- [1] R. Sanchez, J. Mondot, Z. Stankovski, A. Cossic, I. Zmijarevic, "APOLLO II : A User-Oriented, Portable, Modular Code for Multigroup Transport Assembly Calculations," *Nucl. Sci. Eng.*, **100**, p. 352 (1988).
- [2] E. Lewis, W. Miller, *Computational Methods of Neutron Transport*, John Wiley & Sons, NY (1984).
- [3] R. Sanchez, A. Chetaine, "A Synthetical Acceleration for Two-Dimensional Characteristics Method in Unstructured Meshes," *Nucl. Sci. Eng.*, **136**, pp. 122–139 (2000).
- [4] M. Halsall, "CACTUS: A Characteristics solution to the neutron transport equations in complicated geometries," *AEEW-R-1291*, Atomic Energy Establishment, UK (1980).
- [5] L. Goldberg, J. Vujic, A. Leonard, R. Stachowski, "The Characteristics Method in General Geometry," *Trans. Am. Nucl. Soc.*, **73**, pp. 173–174 (1995).
- [6] M. Adams, E. Larsen, "Fast Iterative Methods for Discrete-Ordinates Particle Transport Calculations," *Prog. Nucl. Energy*, **40**, pp. 3–159 (2002).
- [7] G. Grassi, "A Non-linear Spatial Multigrid Acceleration for the Method of Acceleration of the Characteristics in Unstructured Meshes," *International Topical Meeting on Mathematics and Computation, Supercomputing, Reactor Physics and Nuclear and Biological Applications*, Avignon, France (2005).
- [8] R. Sanchez, L. Mao, S. Santandrea, "Treatment of boundary conditions in trajectory-based deterministic transport methods," *Nucl. Sci. Eng.*, **140**, pp. 23–50 (2002).
- [9] P. Wesseling, *An Introduction to Multigrid Methods*, John Wiley & Sons, Chichester, England (1992).
- [10] W. Hackbusch, *Multi-Grid Methods and Applications*, Springer-Verlag, Heidelberg, Germany (1985).
- [11] K. Smith, J. Rhodes, "Full-Core, 2-D, LWR Core Calculations with CASMO-4E," *PHYSOR 2002*, Seoul, Korea (2002).
- [12] K. Koebke, "A new approach to homogenization and group condensation," *IAEA-TECDOC*, International Atomic Energy Agency, Vol. 231, p. 303 (1978).
- [13] K. Koebke, "Advances in homogenization and dehomogenization," *Internal Topical Meeting on Advances in Mathematical Methods for the Solution of Nuclear Engineering Problems*, Munich, 27-29 April, Vol. 2, p. 59 (1981).

- [14] H. Joo, J. Cho, H. Kim, S. Zee, M. Chang, "Dynamic Implementation of the Equivalence Theory in the Heterogeneous Whole Core Transport Calculation," *PHYSOR 2002*, Seoul, Korea (2002).
- [15] S. Nakamura, *Computational Methods in Engineering and Science*, John Wiley & Sons, NY (1977).
- [16] E. Wachspress, *Iterative Solutions of Elliptic Systems and Applications to the Neutron Diffusion Equations of Reactor Physics*, Prentice-Hall Inc., Englewood Cliffs, N.J. (1966).
- [17] AEN-NEA, "Physics of Plutonium Recycling. Vol. VII," BWR MOX Benchmark Specifications and Results (2003).
- [18] A. Aggery, L. Buiron, "Étude du Benchmark d'un assemblage REB de type MOX Atrium 10," Internal note.
- [19] A. Leonard, C. T. McDaniel, "Optimal Polar Angles and Weights for the Characteristics Method," *Trans. Am. Nucl. Soc.*, **73**, pp. 172–173 (1995).
- [20] AEN-NEA, "Expert Group on 3-D Radiation Transport Benchmarks," Benchmark Specification for 2-D/3-D MOX Fuel Assembly Transport Calculations without Spatial Homogenization (C5G7MOX) (2001).
- [21] S. Santandrea, R. Sanchez, "Acceleration technique for the method of characteristics in unstructured meshes," *Annals of Nuclear Energy*, **29**, pp. 323–352 (2002).
- [22] S. Santandrea, Private Communication.

List of Figures

- 1 Fine and coarse spatial discretisations of a given domain \mathcal{D} . The coarse discretisation is obtained from the fine one by an agglomeration procedure. Each macro-region \mathcal{D}_I is defined as the union of a number of fine regions \mathcal{D}_i 30
- 2 Visualisation of V-Cycle scheme for the acceleration of the inner iterations. 31

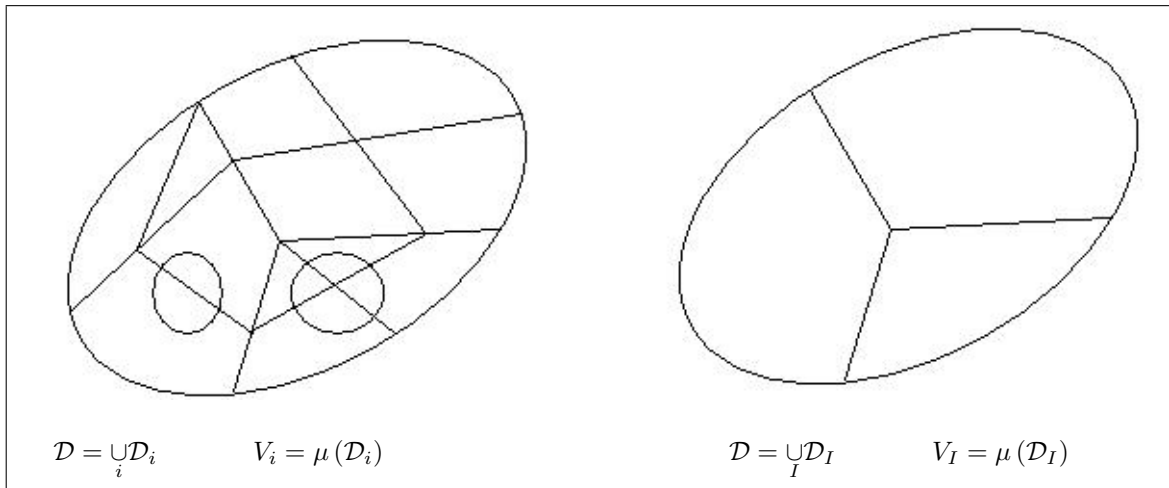


Figure 1: Fine and coarse spatial discretisations of a given domain \mathcal{D} . The coarse discretisation is obtained from the fine one by an agglomeration procedure. Each macro-region \mathcal{D}_I is defined as the union of a number of fine regions \mathcal{D}_i .

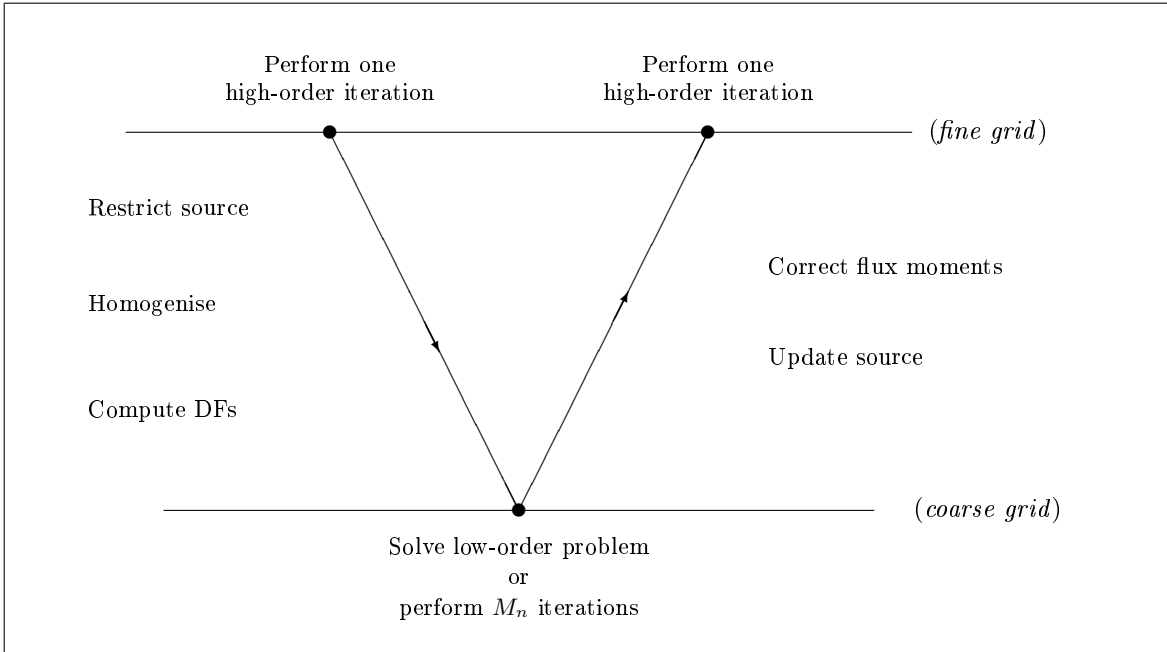


Figure 2: Visualisation of V-Cycle scheme for the acceleration of the inner iterations.

Table I: Atrium Benchmark. Tracking parameters for the fine level. The number of tracks is the total number of intersections of trajectories with regions.

Regions	Azimuthal angles	Polar angles	Spacing (cm)	Trajectories	Tracks
3052	20 (uniform)	3 (Bickley)	0.02	1084	954,466

Table II: Atrium Benchmark. Tracking parameters for the coarse level. Two cases are presented. In the first the same set of trajectories as on the fine level is used. In the second a coarser angular representation and a bigger spacing between parallel trajectories are used.

Case	Regions	Azimuthal angles	Polar angles	Spacing (cm)	Trajectories	Tracks
Spatial MG	136	20 (uniform)	3 (Bickley)	0.02	1084	161,222
Space-Angle MG	136	4 (uniform)	2 (Bickley)	0.06	113	11,301

Table III: Results for the Atrium assembly benchmark with the same set of trajectories on both levels. All times are expressed in seconds.

$k_{eff} = 1.12854$	Free	Space MG	
		Only Inner	Inner & Thermal
building time	5.85	7.33	7.27
solving time	555.24	138.97	149.08
(fine+coarse+other)		(54.44+48.11+36.42)	(30.78+89.52+28.78)
total time	561.09	146.30	156.35
# transport sweeps	1403	103	64

Table IV: Results for the Atrium assembly benchmark using the space-angle two-level acceleration method. All times are expressed in seconds. Two batches of results are presented: for the not-initialised and the initialised case.

$k_{eff} = 1.12854$		Free	Space-Angle MG	
			Only Inner	Inner & Thermal
Not initialised	building time	5.85	4.22	4.25
	solving time	555.24	62.39	45.93
	(fine+coarse+other)		(46.05+2.36+13.98)	(28.61+4.59+12.74)
	total time	561.09	66.61	50.18
	# transport sweeps	1403	103	64
Initialised	building time		4.11	4.15
	initialising time		3.33	4.80
	solving time		45.12	27.65
	(fine+coarse+other)		(30.24+2.68+12.20)	(18.64+4.93+4.08)
	total time		52.56	36.60
	# transport sweeps		64	40

Table V: C5G7MOX Benchmark. Tracking parameters for fine and coarse levels.

Level	Regions	Azimuthal angles	Polar angles	Spacing (cm)	Trajectories	Tracks
Fine	19188	8 (uniform)	2 (Bickley)	0.03	5492	2,378,011
Coarse	1414	2 (uniform)	1 (Bickley)	0.09	934	49,400

Table VI: Results for C5G7MOX Benchmark. Our space-angle acceleration method is applied to both inner and outer iterations. We compare our results with an APOLLO2 reference calculation. All times are expressed in seconds.

	APOLLO2 Reference	Space-Angle MG
k_{eff}	1.18647	1.18637
building time	85.89	17.70
initialisation time	15.86	21.74
solving time	37.50	103.22
(fine+coarse+other)	—	(23.94+64.34+14.94)
total time	139.25	142.66
# transport sweeps	28	35
# outer iterations	4	5